J Appl Physiol 295: 1916–1926, 2008.
First published August 21, 2008; doi:10.1152/japplphysiol.90572.2008.

Hemodynamic impact of mitral prosthesis-patient mismatch on pulmonary hypertension: an in silico study

David Tanné,[1,2] Lyes Kadem,[3] Régis Rieu,[2] and Philippe Pibarot[1]

[1]*Quebec Heart Institute/Laval Hospital, Laval University, Sainte-Foy, Québec,* [3]*Department of Mechanical and Industrial Engineering, Concordia University, Montreal, Quebec, Canada; and* [2]*Cardiovascular Biomechanics Team, Institut de Recherche sur les Phénomènes Equilibre, Centre National de Recherche Scientifique, Université de la Méditerranée, Marseille, France*

Submitted 25 April 2008; accepted in final form 18 August 2008

Tanné D, Kadem L, Rieu R, Pibarot P. Hemodynamic impact of mitral prosthesis-patient mismatch on pulmonary hypertension: an in silico study. *J Appl Physiol* 295: 1916–1926, 2008. First published August 21, 2008; doi:10.1152/japplphysiol.90572.2008.—Recent clinical studies reported that prosthesis-patient mismatch (PPM) becomes clinically relevant when the effective orifice area (EOA) indexed by the body surface area (iEOA) is $<$1.2–1.25 cm^2/m^2. To examine the effect of PPM on transmitral pressure gradient and left atrial (LA) and pulmonary arterial (PA) pressures and to validate the PPM cutoff values, we used a lumped model to compute instantaneous pressures, volumes, and flows into the left-sided heart and the pulmonary and systemic circulations. We simulated hemodynamic conditions at low cardiac output, at rest, and at three levels of exercise. The iEOA was varied from 0.44 to 1.67 cm^2/m^2. We normalized the mean pressure gradient by the square of mean mitral flow indexed by the body surface area to determine at which cutoff values of iEOA the impact of PPM becomes hemodynamically significant. In vivo data were used to validate the numerical study, which shows that small values of iEOA (severe PPM) induce high PA pressure (residual PA hypertension) and contribute to its nonnormalization following a valve replacement, providing a justification for implementation of operative strategies to prevent PPM. Furthermore, we emphasize the major impact of pulmonary resistance and compliance on PA pressure. The model suggests also that the cutoff iEOA that should be used to define PPM at rest in the mitral position is ~1.16 cm^2/m^2. At higher levels of exercise, the threshold for iEOA is rather close to 1.5 cm^2/m^2. Severe PPM should be considered when iEOA is $<$0.94 cm^2/m^2 at rest.

heart valve; mitral flow; lumped model; pulmonary resistance; effective orifice area

IN PATIENTS WITH SEVERE MITRAL valve disease, it is generally well accepted that it is preferable to repair, rather than replace, the valve. Indeed, mitral valve replacement (MVR) has higher short- and long-term mortality than aortic valve replacement or mitral valve repair (9). Unfortunately, in a substantial proportion of patients, the valve cannot be repaired and, thus, needs to be replaced by a prosthetic valve. The suboptimal results of MVR underline the importance of identifying and, whenever possible, preventing prosthesis- and patient-related factors associated with negative hemodynamic and clinical outcomes.

Prosthesis-patient mismatch (PPM) occurs when the effective orifice area (EOA) of the prosthesis is too small relative to the patient's body size, resulting in an abnormally high postoperative pressure gradient. The parameter that is generally used to identify PPM is, thus, the EOA of the prosthesis indexed for the patient's body surface area (BSA) (6, 7, 27). The rationale behind the normalization of EOA for BSA is to account for cardiac output (CO) requirements, since transvalvular pressure gradients are essentially determined by EOA and transvalvular flow, which in turn are largely determined by body size.

In the mitral position, PPM can be equated to residual mitral stenosis (MS) with similar consequences, i.e., the persistence of abnormally high mitral pressure gradients and increased left atrial (LA) and pulmonary arterial (PA) pressures (19). In turn, PA hypertension may cause right-sided failure, and the persistence of high LA pressures may predispose to atrial fibrillation (23).

In contrast to aortic PPM, the hemodynamic and clinical impact of PPM after MVR has been relatively unexplored (7, 8, 29). In particular, the cutoff values that should be used to identify mitral PPM and quantify its severity are controversial. In the early 1990s, Dumesnil et al. (7, 8) demonstrated a relationship between indexed EOA (iEOA) and the transvalvular pressure gradient in normally functioning prostheses implanted in the mitral position. They suggested that mitral PPM occurs when iEOA is $<$1.3–1.5 cm^2/m^2. Two recent clinical studies (16, 21) in a large series of patients reported that PPM, defined as iEOA $<$1.2–1.25 cm^2/m^2, is associated with less regression of PA hypertension, less freedom from heart failure, and reduced survival. One of these studies (21) also showed that the impact of PPM on postoperative mortality becomes significant when iEOA is $\leq$0.9 cm^2/m^2. This level of iEOA was referred to as severe mitral PPM.

The effect of PPM on PA pressure is also not completely known. Although PPM is associated with a high mitral pressure gradient, the parameters that determine the passive elevation of PA pressure are relatively unexplored. Recently, in a retrospective study of 53 patients who underwent MVR, we observed a good correlation between iEOA and systolic PA pressure (19). Moreover, the patients generally had persistent PA hypertension when iEOA was $\leq$1.2 cm^2/m^2, suggesting a significant impact of PPM on PA pressure.

Lumped models are widely used in the cardiovascular domain. They are not time consuming, and they allow prediction of physiological and pathological pressure, volume, and flow waveforms. Whereas some models are closed loops (20, 32, 35) to study, for instance, the left ventricular (LV)-right ven-

Address for reprint requests and other correspondence: P. Pibarot, Quebec Heart Institute, Laval Hospital, 2725 Chemin Sainte-Foy, Sainte-Foy, PQ, Canada G1V 4G5 (e-mail: philippe.pibarot@med.ulaval.ca).

The costs of publication of this article were defrayed in part by the payment of page charges. The article must therefore be hereby marked "*advertisement*" in accordance with 18 U.S.C. Section 1734 solely to indicate this fact.

tricular interaction, others deal with a specific cardiac compartment. Garcia et al. (13) developed a ventricular vascular coupling model to study aortic stenosis implications. Sun et al. (33) explored the mitral and pulmonary venous flow patterns according to age and decreased LV contractility, and their findings fitted well with Doppler-echocardiographic measurements. Recently, two studies attempted to define time dependence of the area in the mitral valve model. Szabo et al. (34) used a second-order forced oscillatory differential equation to derive instantaneous valve area. Korakianitis and Shi (15), using the leaflet inertial moment of rotating and external forces, especially including the vortex effect on the leaflet rotation, computed the angular position of the leaflets of a mechanical prosthesis.

With use of such lumped models, the objective of this numerical study is to examine the effect of mitral iEOA, which is inversely related to the degree of PPM, on transmitral pressure gradient and LA and PA pressures. We used data from a previous clinical study (19) to validate our numerical model. We sought to explain the relationship between iEOA and LA and PA pressures and to determine the most appropriate cutoff iEOA values for identification of moderate and severe PPM in the mitral position on the basis of fluid mechanics considerations.

Glossary

MVR	Mitral valve replacement
PPM	Prosthesis-patient mismatch
MS	Mitral stenosis
VC	Vena contracta
LA	Left atrial
PA	Pulmonary arterial
BSA	Body surface area in m^2
HR	Heart rate in beats/min
EOA	Valve or prosthesis effective orifice area in cm^2
iEOA	EOA indexed by the BSA in cm^2/m^2
M_{mv}	Mitral inertance in g/cm^2
ρ	Constant and uniform fluid density (1.06 g/ml)
SV	Stroke volume in ml
CO	Cardiac output in l/min
CI	Indexed cardiac output in $l \cdot min^{-1} \cdot m^{-2}$
$\tilde{v}_{VC}$	Root-mean-square velocity in the VC in m/s
$Q_{puv}(t)$	Instantaneous pulmonary valve flow (input condition) in ml/s
$\bar{Q}_{puv}$	Mean pulmonary valve flow in ml/s
$\hat{Q}_{puv}$	Peak pulmonary valve flow in ml/s
$Q_{pc}(t)$	Instantaneous pulmonary capillary flow in ml/s
$Q_{pv}(t)$	Instantaneous pulmonary vein flow in ml/s
$Q_{mv}(t)$	Instantaneous mitral valve flow in ml/s
$\bar{Q}_{mv}$	Diastolic mean mitral valve flow in ml/s
$\tilde{Q}_{mv}$	Diastolic root-mean-square mitral valve flow in ml/s
$Q_{av}(t)$	Instantaneous aortic valve flow in ml/s
$Q_{sc}(t)$	Instantaneous systemic capillary flow in ml/s
iQ^2_{mv}	Square of mean mitral flow indexed by BSA in $ml^2 \cdot s^{-2} \cdot m^{-4}$
$i\tilde{Q}^2_{mv}$	Square of root-mean-square mitral flow indexed by BSA in $ml^2 \cdot s^{-2} \cdot m^{-4}$
$\Delta p_{mv}(t)$	Instantaneous maximal transmitral pressure drop (gradient) in mmHg
$\bar{\Delta}\bar{p}_{mv}$	Diastolic mean maximal transmitral pressure drop (gradient) in mmHg
$\hat{\Delta}p_{mv}$	Diastolic peak maximal transmitral pressure drop (gradient) in mmHg
$\Delta p_{av}(t)$	Instantaneous net aortic pressure drop (gradient) in mmHg
K	Normalized mitral pressure gradient ($\bar{\Delta}\bar{p}_{mv}/i\bar{Q}^2_{mv}$) in $mmHg \cdot ml^{-2} \cdot s^2 \cdot m^4$
α	Ratio of mean to root-mean-square mitral flow ($\bar{Q}_{mv}/\tilde{Q}_{mv}$)
$P_{pa}(t)$	Instantaneous pulmonary arterial pressure in mmHg
$\bar{P}_{pa}$	Mean PA pressure in mmHg
$\hat{P}_{pa}$	Systolic peak PA pressure in mmHg
$P_{pvc}(t)$	Instantaneous pulmonary vein and capillary pressure in mmHg
$P_{la}(t)$	Instantaneous LA pressure in mmHg
$\bar{P}_{la}$	Diastolic mean LA pressure in mmHg
$P_{lv}(t)$	Instantaneous LV pressure in mmHg
$P_{ao}(t)$	Instantaneous aortic pressure in mmHg
$P_{svc}(t)$	Instantaneous systemic vein and capillary pressure in mmHg
P_{cv_o}	Constant central venous pressure (output condition; 4 mmHg)
$V_{lv}(t)$	Instantaneous LV volume in ml
$V_{la}(t)$	Instantaneous LA volume in ml
t_{ee}	End-ejection time in s
t_{ar}	LA relaxation time in s
t_{ac}	LA contraction time in s
t_r	Cardiac period in s
T_{mvo}	Mitral valve opening time in s
T_{mvf}	Mitral valve closing time in s
DFT	Diastolic filling time in s
$E_{lv_{es}}$	End-systolic LV elastance in mmHg/ml
$E_{lv_{ed}}$	End-diastolic LV elastance in mmHg/ml
$E_{la_{es}}$	End-systolic LA elastance in mmHg/ml
$E_{la_{ed}}$	End-diastolic LA elastance in mmHg/ml
C_{pa}	Pulmonary arterial compliance in ml/mmHg
C_{pvc}	Pulmonary vein and capillary compliance in ml/mmHg
C_{ao}	Aortic compliance in ml/mmHg
C_{svc}	Systemic vein and capillary compliance in ml/mmHg
R_{pa}	Pulmonary arterial resistance in $mmHg \cdot ml^{-1} \cdot s$
R_{pc}	Pulmonary capillary resistance in $mmHg \cdot ml^{-1} \cdot s$
R_{pvc}	Pulmonary vein and capillary resistance in $mmHg \cdot ml^{-1} \cdot s$
D_{LVOT}	Diameter of LV outflow tract in cm
VTI_{LVOT}	Velocity-time integral of flow in LV outflow tract in cm
R_{pv}	Pulmonary vein resistance in $mmHg \cdot ml^{-1} \cdot s$
R_{ao}	Aortic resistance in $mmHg \cdot ml^{-1} \cdot s$
R_{sc}	Systemic capillary resistance in $mmHg \cdot ml^{-1} \cdot s$
R_{svc}	Systemic vein and capillary resistance in $mmHg \cdot ml^{-1} \cdot s$
R_{sv}	Systemic vein resistance in $mmHg \cdot ml^{-1} \cdot s$
R_{VP}	Pulmonary vascular resistance in $mmHg \cdot ml^{-1} \cdot s$
L_{pc}	Pulmonary capillary inertance in $mmHg \cdot s^2 \cdot ml^{-1}$
L_{PV}	Pulmonary vein inertance in $mmHg \cdot s^2 \cdot ml^{-1}$

L_{sc} Systemic capillary inertance in $mmHg \cdot s^2 \cdot ml^{-1}$

METHODS

Given the purpose of the present study, we elected to simulate only the left-sided heart and the pulmonary and systemic circulations. The models of the LV, the aortic valve, and the systemic circulation are required for computation of the LV systolic pressure, although they are not under consideration here.

Eleven state variables (P_{pa}, P_{pvc}, P_{ao}, P_{svc}, Q_{pc}, Q_{pv}, Q_{mv}, Q_{av}, Q_{sc}, V_{la}, and V_{lv}) were computed step-by-step, with their first derivatives used to lead to instantaneous variations in flows, pressures, and volumes. A schematic of the lumped model is presented in Fig. 1.

The APPENDIX relates in detail the output condition and the models describing the aortic valve, the LV and LA volumes and pressures, and the pulmonary and systemic circulations.

Input condition. The model was excited by the pulmonary valve flow [$Q_{puv}(t)$], i.e., the flow ejected by the right ventricle. The shape of $Q_{puv}(t)$ was simplified to an end-ejection time duration (t_{ee}) and peak pulmonary flow ($\hat{Q}_{puv}$) amplitude rectified sine function. The relationship between mean pulmonary flow ($\bar{Q}_{puv}$) and $\hat{Q}_{puv}$ was therefore

$$\bar{Q}_{puv} = \frac{2\hat{Q}_{puv}}{\pi} \quad (1)$$

Mitral valve. The valves were assumed to be prosthetic valves fully open or fully closed according to the sign of the corresponding pressure gradient. Opening and closing kinetics were not taken into consideration in the present study, and the EOAs were assumed to be time independent. The model and size of the prosthesis were ignored, inasmuch as we characterized the valves only by their EOA.

For an unsteady incompressible inviscid flow (where viscous effects are ignored) with a constant and uniform density (ρ, in g/ml), the instantaneous maximal pressure drop across the mitral valve [$\Delta p_{mv}(t)$, in mmHg], named "gradient" in clinical practice, which is the pressure difference between the LA and the vena contracta (VC) of the jet flow downstream of the valve, was described when the mitral valve was opened by the unsteady Bernoulli's law

$$\Delta p_{mv}(t) = P_{la}(t) - P_{vc}(t) = \frac{\rho}{2EOA_{mv}^2} Q_{mv}^2(t) + \frac{M_{mv}}{EOA_{mv}} \frac{dQ_{mv}(t)}{dt} \quad (2)$$

where the velocity in the LA is neglected compared with the velocity in the VC, $Q_{mv}(t)$ is the instantaneous mitral valve flow, and M_{mv} is the inertance as defined by Flachskampf et al. (11).

However, LV pressure does not equal mitral VC pressure because of the pressure recovery phenomenon. Nonetheless, we neglected this pressure recovery component in the present study, because, as opposed to the aortic valve configuration, it is negligible in the mitral valve configuration because of the presence of a much larger chamber (LV vs. aorta) downstream of the valve (38). Moreover, to be clinically relevant, our PPM cutoff values must be derived from Doppler gradients, which correspond to maximal pressure gradients, and not to net mitral pressure gradients.

Parameters used in the simulations. The set of nonlinear coupled differential equations was solved step-by-step (0.2-ms-time step) by a four-order Runge-Kutta method. We iterated the calculations using the final values of the actual cycle as new initial conditions for the next period until two consecutive cycles became periodic; i.e., the root-mean-square error of each state variable did not exceed a precision of 0.01%.

Table 1 shows the parameters that are held fixed for the present study. The values are determined according to the work of Sun et al. (33) or the achievement of physiological pressure, volume, and flow waveforms at rest.

An input rectified sine function for $Q_{puv}(t)$ and *Eq. 1* allowed us to directly control the stroke volume (SV) by $\hat{Q}_{puv}$ as follows

$$SV = t_{ee}\bar{Q}_{puv} = \frac{2t_{ee}}{\pi}\hat{Q}_{puv} \quad (3)$$

where t_{ee} is the systolic ejection time. Defining a desired diastolic filling time (DFT) according to heart rate (HR) from Lespeschkin (17), one can define t_{ee} as $t_r - DFT$, where t_r is the cardiac period. Mean transmitral flow ($\bar{Q}_{mv}$) was therefore

$$\bar{Q}_{mv} = \frac{SV}{DFT} = \frac{2t_{ee}}{\pi DFT}\hat{Q}_{puv} \quad (4)$$

CO was also determined by $\hat{Q}_{puv}$

$$CO = \frac{SV \cdot HR}{1{,}000} = \frac{t_{ee}HR}{500\pi}\hat{Q}_{puv} \quad (5)$$

Finally, defining the normal cardiac index (CI), which reflects the normal CO requirements according to HR, we can deduce the simulated BSA by dividing CO by CI

$$BSA = \frac{t_{ee}HR}{500\pi CI}\hat{Q}_{puv} \quad (6)$$

From *Eq. 2*, the two main parameters that determine the mean and the peak pressure difference (inertial term null) are the EOA and the mitral root-mean-square flow ($\bar{Q}_{mv}$). Inasmuch as our objective was to determine the relationship between pressure gradients and iEOA, it was necessary to hold $\bar{Q}_{mv}$ constant during the computation to inhibit confounding effects. In a first approximation, we held constant $\bar{Q}_{mv}$, instead of $\bar{Q}_{mv}$. The consequences of this choice are described in RESULTS. For a fixed HR, this approximation is equivalent to a constant SV (*Eq. 3*) or a constant CO (*Eq. 5*).

Then, to vary iEOA, we could change EOA or BSA. However, we chose to keep BSA fixed, because, as opposed to EOA, the only way to vary BSA at fixed HR was a proportional variation in $\hat{Q}_{puv}$ (*Eq. 6*). According to *Eq. 4*, this implied nonrequired variations in $\bar{Q}_{mv}$.

Therefore, we simulated a patient (fixed BSA = 1.8 m^2) at rest (HR = 70 beats/min, $\bar{Q}_{mv}$ = 163 ml/s) and at three levels of exercise [HR = 90 beats/min, $\bar{Q}_{mv}$ = 234 ml/s (mild); HR = 110 beats/min, $\bar{Q}_{mv}$ = 316 ml/s (moderate); HR = 130 beats/min, $\bar{Q}_{mv}$ = 398 ml/s (strenuous)]. For each level of HR, we varied the mitral valve EOA (range 0.8–3.0 cm^2, 0.1-cm^2 step), resulting in iEOA variations from 0.44 to 1.67 cm^2/m^2. An additional simulation (iEOA = 0.28–1.33 cm^2/m^2) was carried out to account for patients in a low-CO state (HR = 50 beats/min, $\bar{Q}_{mv}$ = 103 ml/s). Table 2 shows the simulated parameters. In the aortic position, no PPM existed, since aortic iEOA

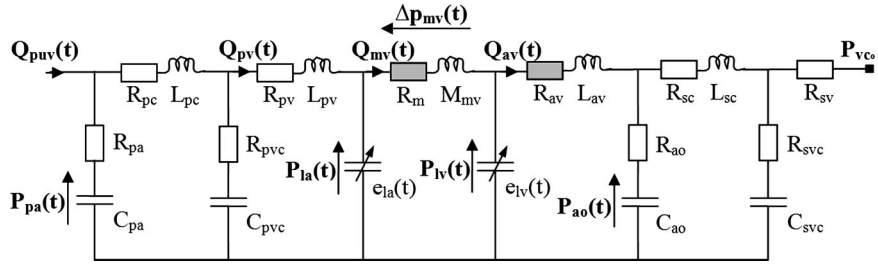

Fig. 1. Lumped model used to simulate left-sided heart and pulmonary and systemic circulations. See *Glossary* for abbreviations.

Table 1. *Fixed parameters used to simulate all cases*

Pulmonary circulation	R_{pa}, mmHg·s·ml^{-1}	R_{pc}, mmHg·s·ml^{-1}	R_{pvc}, mmHg·s·ml^{-1}	R_{pv}, mmHg·s·ml^{-1}	C_{pa}, ml/mmHg	C_{pvc}, ml/mmHg	L_{pc}, mmHg·s^2·ml^{-1}	L_{pv}, mmHg·s^2·ml^{-1}
	0.01	0.21	0.01	0.002	2	40	0.0003	0.0005
LA elastance	$E_{la_{es}}$, mmHg/ml	$E_{la_{ed}}$, mmHg/ml	τ_{lac}, ms	τ_{lar}, ms				
	0.065	0.055	50	50				
LV elastance	$E_{lv_{es}}$, mmHg/ml	$E_{lv_{ed}}$, mmHg/ml	τ_{lvr}, ms	T_{lvr}, ms				
	2.1	0.06	20	600				
Mitral valve	M_{mv}, g/cm^2							
	0.53							
Aortic valve	EOA_{av}, cm^2	A_{ao}, cm^2						
	1.7	5						
Systemic circulation	R_{ao}, mmHg·s·ml^{-1}	R_{sc}, mmHg·s·ml^{-1}	R_{svc}, mmHg·s·ml^{-1}	R_{sv}, mmHg·s·ml^{-1}	C_{ao}, ml/mmHg	C_{svc}, ml/mmHg	L_{sc}, mmHg·s^2·ml^{-1}	
	0.05	0.1	0.01	0.8	0.5	2	0.0005	
Output	P_{cv_0}, mmHg							
	4							
	Time Step, ms	ρ, g/ml						
Other	0.2	1.06						

See *Glossary* for abbreviations.

was 0.94 cm^2/m^2. $\hat{Q}_{puv}$ was calculated according to *Eq. 3* (range 325–679 ml/s).

Measurements on the simulated data. Several clinical indexes can be derived from the simulated instantaneous pressures, volumes, and flows. Timing of mitral valve opening (T_{mvo}) and timing of mitral valve closure (T_{mvf}) corresponding to the gradient inversion were used to measure the simulated DFT. SV was calculated as the difference between LV end-diastolic volume ($V_{lv_{ed}}$) and LV end-systolic volume ($V_{lv_{es}}$). The resulting CO was the ratio of SV to the simulated DFT. $\overline{\Delta p}_{mv}$, $\bar{P}_{la}$, $\bar{P}_{lv}$, and $\bar{Q}_{mv}$ were the averages of each variable only over the simulated DFT, whereas $\bar{P}_{pa}$ is the average over the entire period. $\hat{P}_{pa}$ was the peak value of the PA pressure.

In vivo validation. We used previously published in vivo data from our laboratory (19) to validate our numerical model. In our previous study, 56 patients (65 ± 12 yr old) were evaluated by Doppler echocardiography at the Quebec Heart Institute. Mitral valve EOA was determined by the continuity equation. Peak and mean mitral valve gradients were derived from the simplified Bernoulli's equation. Inasmuch as the mean gradient was calculated from the instantaneous mitral flow velocity (in m/s) at the VC obtained by the Doppler-echocardiographic system and with the assumption that, as the first approximation, EOA did not depend on time, $\tilde{Q}_{mv}$ (in ml/s) can be estimated as

$$\overline{\Delta p}_{mv} = 4\tilde{v}_{vc}^2 = \frac{4}{10{,}000}\frac{\tilde{Q}_{mv}^2}{EOA_{mv}^2} \quad \Rightarrow \quad \tilde{Q}_{mv} = 50\sqrt{\overline{\Delta p_{mv}}}EOA_{mv} \tag{7}$$

The echocardiographic mean mitral flow ($\bar{Q}_{mv}$) was calculated as

$$\bar{Q}_{mv} = \frac{SV}{DFT} = \frac{\pi D_{LVOT}^2 VTI_{LVOT}}{4DFT} \tag{8}$$

where D_{LVOT} and VTI_{LVOT} are the diameter of the LV outflow tract (LVOT), which was assumed to be circular, and the velocity-time integral of the flow in the LVOT, respectively.

Sensitivity analysis. The sensitivity of the model to some critical parameters was also examined. We studied the change in $\bar{Q}_{mv}$, the ratio $\tilde{Q}_{mv}/\bar{Q}_{mv}$, $\overline{\Delta p}_{mv}$, $\hat{\Delta}p_{mv}$, $\bar{P}_{la}$, $\bar{P}_{lv}$, $\bar{P}_{pa}$, and $\hat{P}_{pa}$ according to left cardiac cavity contractility ($E_{lv_{ed}}$, $E_{lv_{es}}$, $E_{la_{ed}}$, and $E_{la_{es}}$), pulmonary resistance (R_{pc} and R_{pv}) and compliance (C_{pa} and C_{pvc}), systemic resistance (R_{sc} and R_{sv}) and compliance (C_{ao} and C_{svc}), CO ($\hat{Q}_{puv}$ with *Eq. 5*), mitral inertance (M_{mv}), and aortic and mitral EOA (EOA_{av} and EOA_{mv}). Each of these parameters was varied between +25% and −25% of its reference value listed in Table 1. For mitral EOA, two different values, which correspond to the severe and

Table 2. *Parameters used for simulating a patient at rest and during mild, moderate, and strenuous exercise*

	HR, beats/min	t_r, ms	CI, l·min^{-1}·m^{-2}	CO, l/min	SV, ml	DFT, ms	$\bar{Q}_{mv}$, ml/s	i$\bar{Q}_{mv}$, ml·s^{-1}·m^{-2}	t_{ee}, ms	t_{ac}, ms	t_{ar}, ms	$\hat{Q}_{puv}$, ml/s
Low CO	50	1,200	2.3	4.1	82.8	800	103	57.5	400	1,050	1,300	325
Rest	70	857	3.3	5.9	84.9	520	163	90.7	337	770	900	396
Exercise												
Mild	90	666	4.5	8.1	90	385	234	130	281	600	700	503
Moderate	110	545	5.8	10.4	94.9	300	316	175.8	245	510	600	609
Strenuous	130	461	6.9	12.4	95.6	240	398	221.2	221	410	490	679

BSA = 1.8 m^2. See *Glossary* for abbreviations. HR, CI, DFT, t_{ac}, and t_{ar} values were used to calculate other values.

moderate mismatch cutoff values we found in RESULTS, were set as reference. For the resistances and compliances, the two parameters were varied simultaneously.

RESULTS

Typical volume, pressure, and flow waveforms at rest are displayed in Fig. 2. The model provides realistic patterns for all the state variables.

Influence of iEOA on mitral gradient. Mean and peak mitral pressure gradient values are depicted in Fig. 3, *A* and *B*. Theoretically, the inertial term becomes null, if we take the diastolic average or the peak instant of *Eq. 2*, so that the pressure gradients depend only on EOA and $\tilde{Q}_{mv}$. Figure 3 is therefore a simple representation of *Eq. 2*: the pressure gradients increase as EOA decreases and $\tilde{Q}_{mv}$ increases.

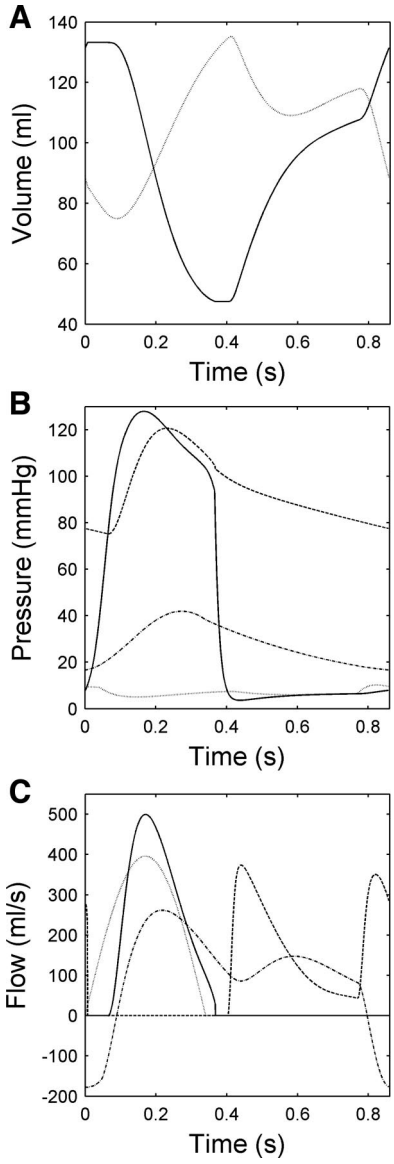

Fig. 2. Typical LA (dotted line) and LV (solid line) volumes (*A*), aortic (dashed line), LV (solid line), PA (dashed-dotted line) and LA (dotted line) pressures (*B*), and aortic valve (solid line), mitral valve (dashed line), pulmonary valve (dotted line) and pulmonary venous (dashed-dotted line) flows (*C*) at rest (HR = 70 beats/min). Parameters are listed in Tables 1 and 2. Mitral effective orifice area (EOA) was set to 4 cm^2.

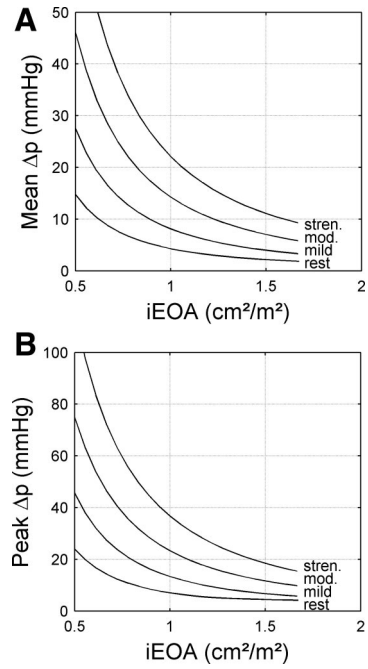

Fig. 3. Mean (*A*) and peak (*B*) maximal mitral pressure gradient (Δp) vs. indexed EOA (iEOA) at rest and during mild, moderate (mod), and strenuous (stren) exercise.

Correlation between $\bar{Q}_{mv}$ and $\tilde{Q}_{mv}$. To explore the a priori unknown relationship between $\bar{Q}_{mv}$ and $\tilde{Q}_{mv}$, we have plotted in Fig. 4 the results for three HRs (50, 70, and 90 beats/min).

First, $\bar{Q}_{mv}$ does not remain constant at fixed HR, in contrast to the prediction from *Eq. 4*. This can be explained by the fact that simulated DFT changes according to iEOA, independently of HR. Figure 5 shows the mitral flow pattern at rest for three different mitral EOA values. When EOA decreases, not only is the amplitude of E and A waves reduced, but DFT increases as well. Indeed, mitral opening and closing times are entirely due to the sign of the pressure gradient, which is not fixed in these simulations but is controlled by *Eq. 2*. Inasmuch as SV is fixed by *Eq. 3*, $\bar{Q}_{mv}$ decreases.

The shapes of the three $\bar{Q}_{mv}$-$\tilde{Q}_{mv}$ curves constructed at three different HRs are similar and can be divided into two portions: the first portion (upper part of the curves) shows a quasi-constant $\bar{Q}_{mv}$ while $\tilde{Q}_{mv}$ increases progressively. This portion corresponds to the simulated data for large iEOAs, where the

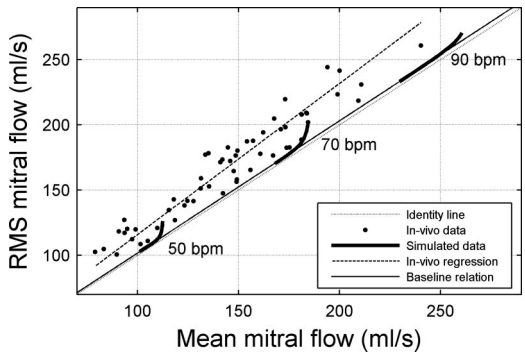

Fig. 4. Mean mitral flow vs. root-mean-square (RMS) mitral flow. Baseline relation is *Eq. 9*; in vivo regression corresponds to *Eq. 10*. bpm, Beats per minute.

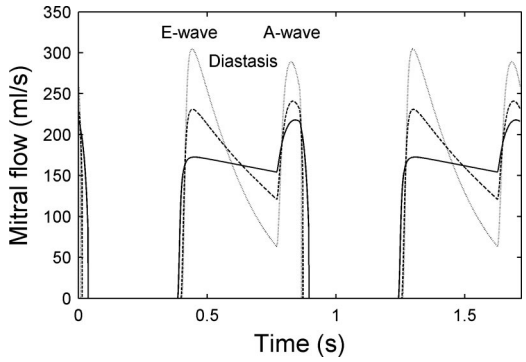

Fig. 5. Mitral flow pattern at 70 beats/min for mitral EOA = 0.8 cm^2 (solid line), 1.9 cm^2 (dashed line), and 3.0 cm^2 (dotted line).

mitral flow pattern is biphasic, with short E-wave deceleration time and high E- and A-wave amplitudes (Fig. 5; EOA = 3.0 cm^2). These large fluctuations and amplitudes of $Q_{mv}(t)$ are therefore responsible for the differences between $\bar{Q}_{mv}$ and $\tilde{Q}_{mv}$.

On the contrary, the lower parts of the curves exhibit an asymptotic linear behavior, which is characteristic of a highly restrictive orifice (i.e., low iEOA), where the amplitudes of E- and A-flow waves are smaller and the E-flow wave deceleration time is much longer than for large iEOAs (Fig. 5; EOA = 0.8 cm^2). A linear regression without intercept between the last points of the three curves (Fig. 4) gives the following relation: $R^2 = 0.99$, which is different from the identity line

$$\tilde{Q}_{mv_{sim}} = 1.014\bar{Q}_{mv_{sim}} \quad (9)$$

To corroborate these results, we have plotted in Fig. 4 the relationship between $\tilde{Q}_{mv}$ and $\bar{Q}_{mv}$, which are calculated using *Eqs. 7* and *8*, respectively, from previously published in vivo data. No in vivo data points fall below the simulated regression line (*Eq. 9*), thus supporting the notion that there is a baseline relationship between $\tilde{Q}_{mv}$ and $\bar{Q}_{mv}$. For a fixed $\bar{Q}_{mv}$, $\tilde{Q}_{mv}$ cannot be smaller than the value predicted by *Eq. 9,* but it can nonetheless be higher, depending on the shape of the mitral flow. When iEOA increases and, thus, the biphasic pattern of mitral flow becomes more pronounced, $\tilde{Q}_{mv}$ increases to a greater extent than does $\bar{Q}_{mv}$.

In the clinical setting, factors other than the EOA influence the relationship between $\tilde{Q}_{mv}$ and $\bar{Q}_{mv}$ (see *Sensitivity analysis*; see Fig. 8), which explains the variation of the in vivo data. This variation is attenuated for the simulated data because of the use of fixed parameters (Table 1). The baseline relationship (*Eq. 9*) cannot therefore be representative of daily clinical observations. Consequently, we have considered that a regression analysis of the in vivo data better represents the average relationship between $\bar{Q}_{mv}$ and $\tilde{Q}_{mv}$ for a standard cohort for mean mitral flow of 80–240 ml/s. The linear regression without intercept (Fig. 4) provides the following equation ($R^2 = 0.91$)

$$\tilde{Q}_{mv_{vivo}} = 1.159\bar{Q}_{mv_{vivo}} \quad (10)$$

This choice is not a correction for the numerical model, since it is able to reproduce clinical observations but is, rather, a better evaluation of the relationship between $\bar{Q}_{mv}$ and $\tilde{Q}_{mv}$.

PPM cutoff values. To determine the PPM cutoff values, we used the relationship between the mitral pressure gradient and iEOA. We normalized the mean maximal mitral pressure gradient ($\bar{\Delta p}_{mv}$) to the square of the mean mitral valve flow divided or indexed for the patient's BSA ($i\bar{Q}^2_{mv}$). The rationale for this normalization was to compensate for *1*) the interindividual variation in $\bar{Q}_{mv}$ in vivo and *2*) the $\bar{Q}_{mv}$ variations in the simulated data previously mentioned. The aim was therefore to describe a unique relationship between $\bar{\Delta p}_{mv}$ and iEOA. From a theoretical standpoint, it would have been preferable to normalize by $i\tilde{Q}^2_{mv}$, because the diastolic average of *Eq. 2* implied

$$K_{th} = \frac{\overline{\Delta p}_{mv}}{i\tilde{Q}^2_{mv}} = \frac{\rho}{2 \cdot iEOA^2_{mv}} \quad (11)$$

Nonetheless, we chose to use mean flow, because, in contrast to the root-mean-square flow, it is largely used in the clinical setting, and it can be easily and accurately measured by Doppler echocardiography. If we define α as the ratio $\tilde{Q}_{mv}/\bar{Q}_{mv}$, the normalized pressure gradient (K) is equal to

$$K = \frac{\overline{\Delta p}_{mv}}{i\bar{Q}^2_{mv}} \frac{\alpha^2 \rho}{2 \cdot iEOA^2_{mv}} = \alpha^2 K_{th} \quad (12)$$

Figure 6 shows the simulated normalized pressure gradients at low CO, at rest, and at the three levels of exercise. The five curves are superimposed because of the normalization. Indeed, for the simulated data, α is ~1 for the five HRs (mean = 1.036, standard deviation = 0.042) leading to

$$K_{sim} \approx K_{th} \quad (13)$$

In Fig. 6, we also plotted the individual data points of the normalized mean pressure gradient for the 56 patients. The normalized in vivo pressure gradient values are higher than the simulated values. This discrepancy is due to the shift between the simulated *Eq. 9* and in vivo *Eq. 10* root-mean-square flows. For in vivo data, the range of α is 1.038–1.362, which is much higher than for the simulated data. Therefore, for the in vivo normalized pressure gradient, *Eqs. 10* and *12* give

$$K_{vivo} = 1.159^2 \frac{\rho}{2 \cdot iEOA^2_{mv}} = \frac{0.71}{iEOA^2_{mv}} = 1.343K_{th} > K_{sim} \quad (14)$$

Similarly to the relationship between $\bar{Q}_{mv}$ and $\tilde{Q}_{mv}$, *Eq. 14* is

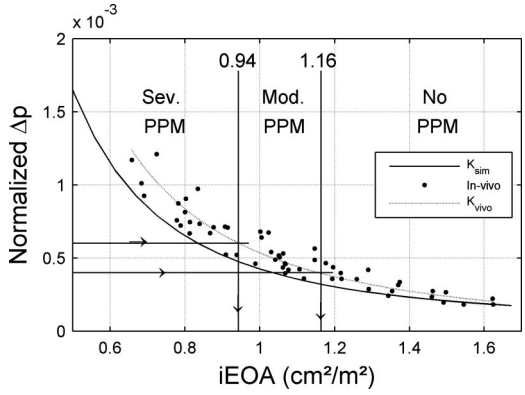

Fig. 6. Mitral pressure gradient normalized to square of the mean mitral valve flow indexed for body surface area (K) vs. iEOA. K in vivo (K_{vivo}, *Eq. 14*) is higher than K in simulated conditions (K_{sim}) because of higher α values in vivo than in silico. PPM, patient-prosthesis mismatch.

not a correction of our numerical model but, rather, is more representative of clinical observations than the simulations described in the present study (see *Limitations of the study*).

Inasmuch as PPM is similar to a residual MS, we have used the hemodynamic severity of this valvular disease to categorize PPM. At rest (i.e., $i\bar{Q}_{mv} = 100$ ml·s^{-1}·m^{-2}), patients with mild and moderate MS generally have mean gradients <5 and >5 mmHg, respectively (2). For a resting mean mitral pressure gradient of 4 mmHg (mild MS), the normalized pressure gradient (*Eq. 14*) is 4.0×10^{-4} mmHg·ml^{-2}·s^2·m^4, which corresponds to iEOA of 1.16 cm^2/m^2 (Fig. 6). The cutoff value of iEOA corresponding to a resting mean mitral pressure gradient of 6 mmHg (moderate MS) is 0.94 cm^2/m^2 (Fig. 6). These results suggest that PPM may have significant hemodynamic impact, i.e., residual MS and high pressure gradient, when iEOA is <1.15–1.20 cm^2/m^2. Hence, this cutoff value would seem appropriate to define clinically significant moderate PPM. Moreover, these results support the notion that PPM is severe when iEOA is ≤0.95 cm^2/m^2. In athlete patients, the objectives in terms of pressure gradient after an MVR are the same as for other patients (3). However, because of their high levels of physical activity, the CO requirement and, thus, the $i\bar{Q}_{mv}$ values are higher for the athlete patients. If a one-third increase ($i\bar{Q}_{mv} = 130$ ml·s^{-1}·m^{-2}) is assumed, the cutoff iEOA for moderate PPM is 1.51 cm^2/m^2 (Fig. 6), suggesting that the prosthesis iEOA should not be <1.5 cm^2/m^2 for an athlete patient.

Impact of PPM on LA and PA pressures. To further explore the hemodynamic impact of PPM defined from the above-mentioned cutoff values, we have plotted the curves of mean LA pressure and mean and systolic PA pressures as a function of iEOA (Fig. 7). The shape of these curves is very similar to the shape of the curves in Fig. 3, except they are shifted toward higher pressure values, in agreement with a passive elevation of PA pressure following an increase in the mitral pressure gradient. According to these simulated curves, $\bar{P}_{la}$ would be >9 mmHg and 10.5 mmHg (+17%) for moderate and severe PPM at rest, respectively. For moderate PPM, $\bar{P}_{pa}$ is >30 and 41 mmHg (+36%) and $\hat{P}_{pa}$ is >44 and 55 mmHg (+25%) at rest and during mild exercise, respectively (Fig. 7). For severe PPM, the values were 31 and 44 mmHg (+42%) for $\bar{P}_{pa}$ and 45 and 58 mmHg (+29%) for $\hat{P}_{pa}$ at rest and during mild exercise, respectively.

Sensitivity analysis. The two main parameters that influence PA pressure are CO and pulmonary vascular resistance ($R_{VP} = R_{pc} + R_{pv}$). Indeed, even if mitral iEOA is sufficiently high to avoid PPM, an increased R_{VP} associated with significant CO is equivalent to a flow obstruction inside the pulmonary circulation and, consequently, an increase in PA pressure with no impact on LA and LV hemodynamics (Fig. 8). Pulmonary compliance also plays an important role, but only on systolic PA pressure, similar to the well-known impact of systemic compliance on aortic pulse pressure. As opposed to LA contractility, which slightly affects LA and PA pressures, an increase of LV end-systolic and end-diastolic elastance values, respectively, decreases and increases mean LV pressure. These variations are echoed directly in LA and PA pressures. Furthermore, when systemic resistance is augmented, not only systolic, but also diastolic, LV pressure increases, which in turn induces an elevation of PA pressure (Fig. 8). However, these results should be interpreted with caution, given that our model does not account for the right heart and control mechanisms, such as the systemic venous compliance, which may act as a buffer. In addition, it does not account for LV diastolic dysfunction, which is frequently associated with hypertensive cardiopathy and may contribute to the development of pulmonary hypertension (10). There is no significant effect of mitral inertance, systemic compliance, aortic valve EOA, and LA end-systolic and end-diastolic elastances.

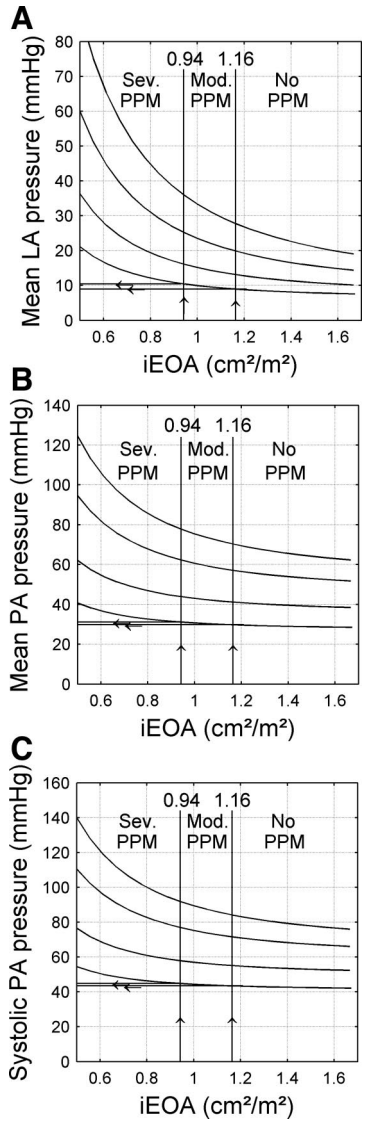

Fig. 7. Mean left atrial (LA) pressure (*A*), mean pulmonary arterial (PA) pressure (*B*), and systolic PA pressure (*C*) vs. iEOA at rest and during mild, moderate, and strenuous exercise.

DISCUSSION

Equation 2 and Fig. 3 clearly demonstrate that the mean transmitral pressure gradient increases nonlinearly with mitral valve EOA. From their in vitro study of the relationship in the aortic and mitral positions, Dumesnil and Yoganathan (8) concluded that a small iEOA is associated with an elevated valve pressure gradient, and they suggested that iEOA should ideally not be <1.3–1.5 cm^2/m^2 in the mitral position. Nevertheless, their diastolic filling period was too short for a normal

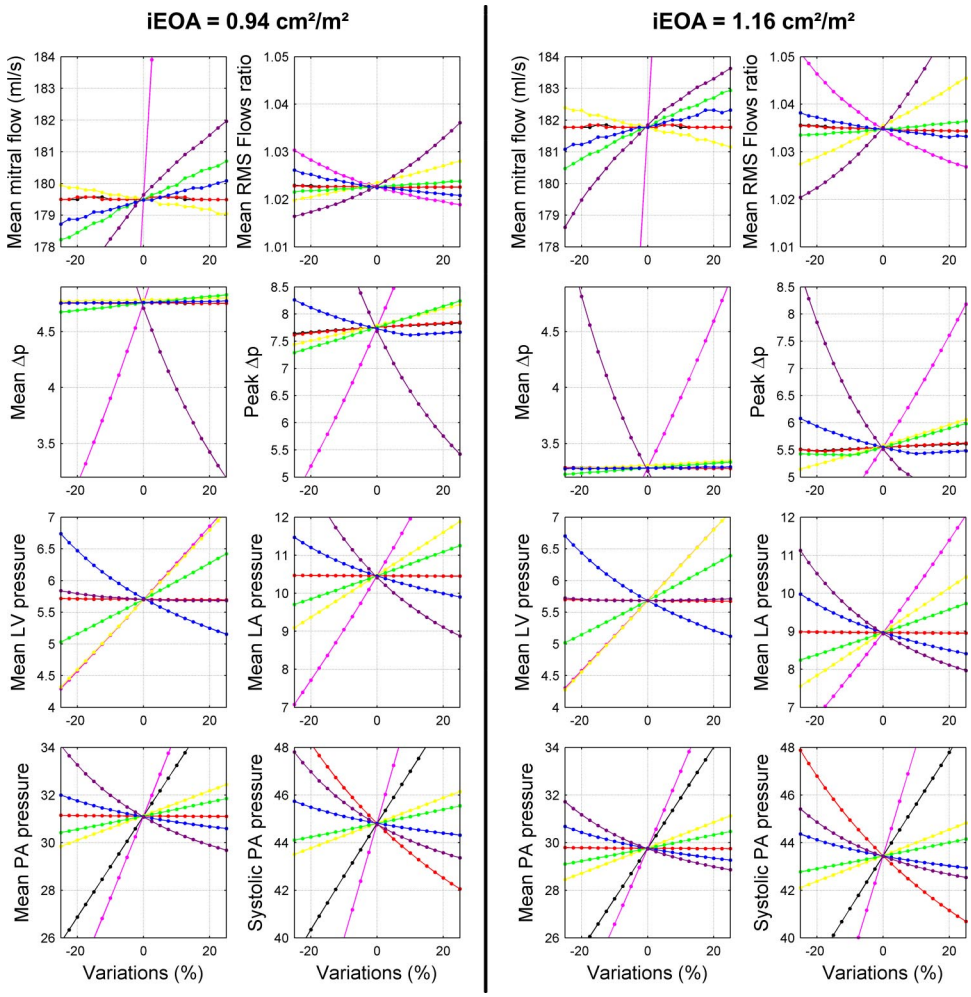

Fig. 8. Results from sensitivity analysis. Each parameter [CO (pink), $E_{lv_{ed}}$ (yellow), $E_{lv_{es}}$ (blue), $R_{pc} + R_{pv}$ (black), $C_{pa} + C_{pvc}$ (red), $R_{sc} + R_{sv}$ (green), and EOA_{mv} (purple)] was varied ±25%.

resting HR and CO. A diastolic filling period of 450–500 ms, which we used in the present study, would have been preferable to 300 ms in their study. This might explain the higher mitral gradients in their study than those simulated in the present study.

In contrast to aortic flow, which can be basically compared with a sine function during the systolic phase, mitral valve flow includes two preponderant waves: the E wave at the beginning of diastole, corresponding to the LV rapid filling, and the A wave, corresponding to the LA end-diastolic contraction. Between these two waves, the flow decreases and is highly patient dependent. This phase, called diastasis, depends on HR (diastasis duration decreases, while HR increases) and on mitral valve EOA (when EOA decreases, amplitudes of E- and A-flow waves decrease and E-wave deceleration time increases). These differences in flow patterns cause large discrepancies (Fig. 4) between the mean flow and the root-mean-square flow, which is much more sensitive to flow variations and amplitudes than the mean flow rate. Using these simulations, we demonstrated a baseline relationship, different from the identity line, between these two flows. Only some patients with high restrictive mitral flow pattern, mainly due to low EOA or high CO, exhibit this baseline relationship. The difference between $\tilde{Q}_{mv}$ and $\bar{Q}_{mv}$ is more important for the rest of the cohort and could explain some discrepancies between catheterization- and Doppler-derived gradient. Further studies are needed to confirm this hypothesis.

Besides the direct impact on transmitral pressure gradients and LA and PA pressures, PPM may also have an indirect impact on pulmonary vascular resistance (R_{VP}). The chronic exposure to elevated PA pressure induces structural modifications of the pulmonary vasculature (hypertrophy of the arterial wall and reduction of the lumen), which in turn contribute to the increase in R_{VP}. The augmentation of R_{VP} further contributes to the increase in PA pressure (Fig. 8), thus initiating a vicious cycle. Hence, patients with mitral stenosis or mitral PPM often have increased R_{VP}. For this reason, in the present study, we used a constant R_{VP} ($R_{pc} + R_{pv}$) of 0.212 mmHg·ml^{-1}·s (3.5 woods), whereas the normal value for a healthy subject is ~1 wood. In clinical practice, pulmonary hypertension is considered to be present at $\bar{P}_{pa} \geq 25$ mmHg or $\hat{P}_{pa} \geq 40$ mmHg at rest and $\hat{P}_{pa} \geq 50$ mmHg during exercise (24). Moderate pulmonary hypertension is defined as $\hat{P}_{pa} \geq 50$ mmHg at rest and $\hat{P}_{pa} \geq 60$ mmHg during exercise and severe pulmonary hypertension as $\hat{P}_{pa} \geq 60$ mmHg at rest (2). Therefore, with R_{VP} of 0.212 mmHg·ml^{-1}·s, we have simulated a patient with moderate PA hypertension.

Although the main goal of MVR is to improve valvular hemodynamics and normalize PA pressure, the results of the present study suggest that impairment of the pulmonary vas-

culature may have an important impact on PA pressure that may outweigh the impact of PPM in some situations. According to Fig. 8, the decrease in PA pressure, i.e., the postoperative regression of pulmonary hypertension, may be hindered by the following factors: *1*) increased R_{VP} and reduced pulmonary compliance due to advanced pulmonary vascular remodeling (12, 18, 22, 26, 37), *2*) postoperative increase in CO due to the normalization of the valvular flow dynamics (5, 39), and *3*) PPM. By maintaining relatively high levels of LA and PA pressures after operation, PPM might interfere with the reversibility of the structural and functional alterations of the pulmonary vasculature and initiates a vicious cycle (27).

The results of the present study also emphasize that, beyond PA pressure, it is important to measure and follow R_{VP} and PA compliance in clinical practice. Indeed, in patients with advanced mitral valve disease, CO may progressively decrease with time, which may, in turn, cause a "pseudonormalization" of PA pressure. Hence, the consideration of PA pressure alone may underestimate the severity of structural and functional impairment of the pulmonary vessels. This is an important limitation, given that, in patients with long-standing disease, potentially irreversible structural changes may occur in the pulmonary vasculature (4, 25). Several methods have been proposed for noninvasive estimation of R_{VP} by Doppler echocardiography (1, 31), and these methods are easily applicable in routine practice. PA compliance can be measured by catheter and is a powerful predictor of outcome in patients with pulmonary hypertension (22). However, this hemodynamic parameter is difficult to estimate by noninvasive methods. In patients with severe mitral valve disease, early operation should eventually be considered in the event of markedly increased R_{VP} or reduced PA compliance, even if the patient is asymptomatic and/or has a $\hat{P}_{pa}$ <50 mmHg. If MVR is performed in these patients, the surgeon should take care to avoid PPM to optimize the normalization of R_{VP} and PA pressure.

Mitral PPM is actually not a new concept. In the first report on mitral PPM published in 1981, Rahimtoola (29) described a patient who remained symptomatic and had persistent PA hypertension and progressive right-sided failure following successful MVR. The only explanation for the persistence of PA hypertension in this patient was a high residual transprosthetic pressure gradient due to PPM, despite a normal functioning prosthesis. Magne et al. (21) used thresholds of 1.2 and 0.9 cm^2/m^2 to define moderate and severe PPM, respectively. The results of the present theoretical study confirm the hemodynamic relevance of the threshold values used in this previous epidemiological study. Lam et al. (16) used a slightly higher threshold for moderate PPM (1.25 cm^2/m^2), but it should be emphasized that they used the geometric orifice area calculated from the internal diameter of the prosthesis or the EOA measured by the pressure half-time method to estimate the EOA of the prosthesis in a substantial proportion of the patients in their series. It has been shown that both methods may overestimate the actual EOA, which may explain why the threshold value selected in their study was somewhat higher than that determined in the present study.

Magne et al. (21) showed that only severe PPM is associated with higher mortality. Indeed, according to Fig. 7, the mean and systolic PA pressures are quasi-constant until the iEOA falls below the cutoff value defining severe PPM. Only very small iEOA (severe PPM) affects the PA pressure, giving a possible explanation of the conclusion of Magne et al.

Hence, two studies from a large series ($n > 800$) of patients published by two independent groups of investigators (16, 21) demonstrated that PPM is frequent after MVR and that it has a significant effect on postoperative regression of PA hypertension, occurrence of heart failure, and survival. Previous studies (7, 8, 19) also demonstrated that the impact of PPM on hemodynamic outcome (i.e., transvalvular gradients and regression of PA hypertension) becomes clinically relevant when iEOA is <1.2–1.3 cm^2/m^2, whereas the impact on survival becomes significant when iEOA is <0.9 cm^2/m^2 (16, 21). Hence, the results obtained in these previous in vivo studies (7, 8, 16, 19, 21) are highly consistent with the results of the present numerical study. In contrast to these results, Totaro and Argano (36) reported that PPM is rare and has no or minimal impact on hemodynamic and clinical outcomes following MVR. This study was, however, based on a small number of patients and had several important limitations that were described in detail in a letter to the editor (28).

Limitations of the study. Our model accurately reproduces the transmitral flow patterns as observed in patients with small iEOAs and short diastasis. However, in patients with longer diastasis and larger iEOAs, the net pressure gradient may become quasi-null and lead to a reduced flow. Therefore, a partial closing of the mitral valve may occur during diastasis and may decrease the instantaneous EOA. In our model, this phenomenon cannot occur, given that the iEOA is fixed throughout diastole. As a consequence, when we simulate patients with long diastasis and a large iEOA, an inversion of the net pressure gradient induces the total closure of the valve during diastasis, which is generally not observed in vivo. This is the main determinant limiting high values of the ratio α (root-mean-square flow ÷ mean flow). Further improvement of our model is thus necessary to provide more realistic mitral valve hemodynamics in the context of large iEOAs. This could be achieved by integrating into the model the time-dependent variation of the mitral EOA and the opening/closing kinetics of the leaflets.

Furthermore, we have simulated five sets of parameters (Table 1) that do not necessarily represent the situation of all the patients in the cohort. With the parameters listed in Table 1, the ratio α is 1.036 for the lower part of each simulated curve (Fig. 4) and increases up to 1.116 (at 50 beats/min), whereas the range for the cohort is 1.038–1.362. According to the sensitivity analysis, α changes not only with iEOA, but also with LA and LV elastances and the properties of the systemic circulation, which therefore could also explain this discrepancy. We thus elected to use α of 1.159 for a better estimation of the PPM thresholds.

This limitation, however, does not affect the results and conclusion of the present study, given that the impact of PPM becomes hemodynamically relevant at lower iEOA values and the performance of our model is good over this range of iEOA values.

Conclusion. This numerical study demonstrates the complex relationship between the mean and root-mean-square mitral flows because of the biphasic mitral flow pattern. The simulations suggest that the cutoff iEOA at which the impact of mitral PPM becomes hemodynamically significant is <1.16 cm^2/m^2. The cutoff iEOA identified in the present study for severe PPM

is <0.94 cm^2/m^2. The results of the present study also suggest that, in athlete patients, the objective should, rather, be to provide an iEOA ≥ 1.5 cm^2/m^2. We emphasize the impact of PPM on LA and PA pressures. The normalization of these pressures following MVR is influenced by the complex interaction between flow rate, PPM, and pulmonary resistance and compliance. Given that PPM is the only factor that is preventable at the time of operation, an effort should be made to apply prospective strategy at the time of operation to avoid PPM or reduce its severity.

APPENDIX

Output condition. The output condition was the central venous pressure P_{cv_0}, which was assumed to be constant throughout the entire cardiac cycle and equal to 4 mmHg.

Aortic valve. In the aortic position, we used the net pressure gradient defined by Garcia et al. (14) to relate the LV and aortic pressures, including the pressure recovery

$$\Delta p_{av}(t) = P_{lv}(t) - P_{ao}(t) = \frac{\rho}{2} Q_{av}^2(t)\left(\frac{1}{EOA_{av}} - \frac{1}{A_{ao}}\right)^2 + 2\pi\rho \frac{dQ_{av}(t)}{dt}\sqrt{\frac{1}{EOA_{av}} - \frac{1}{A_{ao}}}$$

where EOA_{av} and A_{ao} are constant, $EOA_{av} = 1.7$ cm^2, and $A_{ao} = 5$ cm^2, modeling normal aortic valve prosthesis and aorta (14).

Transvalvular flows were then computed from their first derivative as the difference between the pressure gradient and Bernoulli's convective term.

LV and LA volumes and pressures. Using the conservation of mass principle, we can determine cardiac chamber volumes, i.e., LV (V_{lv}) and LA (V_{la}), by

$$\frac{dV_{la}(t)}{dt} = Q_{pv}(t) - Q_{mv}(t) \quad \text{and} \quad \frac{dV_{lv}(t)}{dt} = Q_{mv}(t) - Q_{av}(t)$$

LV pressure was calculated from the time-varying elastance [$E_{lv}(t)$], defined as the instantaneous ratio $P_{lv}(t)/[V_{lv}(t) - V_{lv_0}]$, where V_{lv_0} is the unstressed LV volume and considered constant throughout the entire cardiac cycle. Some authors (15, 33) developed cosine or exponential equations for $E_{lv}(t)$. In 1996, Sensaki et al. (30) described the normalized elastance curves [$E_N(t_N)$], defined as $E_N(t_N) = E_{lv}(t/t_{max})/E_{lv_{max}}$, where $E_{lv_{max}}$ is maximal $E_{lv}(t)$ at t_{max}. They found that $E_{lv_{max}} \cong E_{lv_{es}}$, where $E_{lv_{es}}$ is end-systolic or maximal LV elastance and that these curves were surprisingly similar between a wide range of healthy subjects and ill patients, particularly during early contraction. However, the LV relaxation was more patient dependent (30). Consequently, we modified the normalized function during the relaxation as

$$E'_N(t_N) = \begin{cases} E_N(t_N) & \text{for } 0 < t_N \leq T_{lvr} \\ [E_N(T_{lvr}) - E_N(0)]e^{-\left(\frac{t_N - T_{lvr}}{\tau_{lvr}}\right)} + E_N(0) & \text{for } t_N > T_{lvr} \end{cases}$$

where $T_{lvr} \geq 1$ is the time at which the exponential LV relaxation began. The normalized time constant (τ_{lvr}) controlled for the LV relaxation rate. $E'_N(t_N)$ is a continuous function, but its derivatives, which are not used in the present work, are not. The parameters are as follows: $T_{lvr} = 1.0756$, $\tau_{lvr} = 0.0717$, and $E_N(0) = 0.0758$. The required elastance function was thus an interpolation of $E'_N(t_N)$ at $t_N = t_{ee}$ given by

$$E_{lv}(t) = \text{interp}_{t_N = t_{ee}}[E_{lv_{min}} + E'_N(t_N) * (E_{lv_{es}} - E_{lv_{min}})]$$

where $E_{lv_{min}} = [E_{lv_{ed}} - E_N(0)E_{lv_{es}}]/[1 - E_N(0)]$ and $E_{lv_{ed}}$ is the end-diastolic or minimal LV elastance value. In the first approximation, the LA was considered a pump, so its mathematical description was a delayed [LA contraction (t_{ac}), LA relaxation (t_{ar})] and attenuated ($E_{la_{es}}$, $E_{la_{ed}}$) exponential (τ_{ac}, τ_{ar}) version of the normalized elastance curve.

Pulmonary and systemic circulatory systems. The pulmonary and systemic circulations were modeled as two consecutive four-element windkessel schemes. On one hand, the pulmonary system was divided into pulmonary artery (pa) and mixed capillary-vein (pvc) compliances and into the capillary (pc) and vein (pv) resistances. On the other hand, the systemic circulation consisted of the aorta (ao) and mixed capillary-vein (svc) compliances and the capillary (sc) and vein (sv) resistances.

The time-constant compliance for any chamber (C_k) is given by the relationship between the instantaneous pressure change [$dP_k(t)/dt$] and the difference of the respective instantaneous flow into [$Q_{in}(t)$] and out of [$Q_{out}(t)$] the chamber

$$C_k \frac{dP_k(t)}{dt} = Q_{in}(t) - Q_{out}(t) \quad \text{for} \quad k = \text{pa, pvc, ao, svc}$$

For instance, the instantaneous pulmonary arterial pressure [$P_{pa}(t)$] was calculated as $dP_{pa}(t)/dt = [Q_{puv}(t) - Q_{pc}(t)]/C_{pa}$, where $Q_{pc}(t)$ is pulmonary capillary flow and C_{pa} is pulmonary arterial compliance.

The inertance L_k, accounting for the inertial effect, was described in the same way by a first-order differential equation linking the flow derivative [$dQ_k(t)/dt$] to the upstream pressure [$P_{up}(t)$], the downstream pressure [$P_{down}(t)$], the flow at the node k [$Q_k(t)$], and the vascular Poiseuille's resistance (R_k)

$$L_k \frac{dQ_k(t)}{dt} = P_{in}(t) - P_{out}(t) - R_k Q_k(t) \quad \text{for} \quad k = \text{pc, pv, sc}$$

GRANTS

This work was supported by Canadian Institutes of Health Research Grant MOP 67123 (P. Pibarot). P. Pibarot holds the Canada Research Chair in Valvular Heart Diseases at the Canadian Institutes of Health Research (Ottawa, ON, Canada).

REFERENCES

1. **Abbas AE, Fortuin FD, Schiller NB, Appleton CP, Moreno CA, Lester SJ.** A simple method for noninvasive estimation of pulmonary vascular resistance. *J Am Coll Cardiol* 41: 1021–1027, 2003.
2. **Bonow RO, Carabello B, Chatterjee K, De Leon AC, Faxon DP, Freed MD, Gaasch WH, Lytle BW, Nishimura RA, O'Gara PT, O'Rourke RA, Otto CM, Shah PM, Shanewise JS.** ACC/AHA 2006 guidelines for the management of patients with valvular heart disease. *J Am Coll Cardiol* 48: 1–148, 2006.
3. **Bonow RO, Cheitlin MD, Crawford MH, Douglas PS.** Task Force 3: valvular heart disease. *J Am Coll Cardiol* 45: 1334–1340, 2005.
4. **Cortese DA.** Pulmonary function in mitral stenosis. *Mayo Clin Proc* 53: 321–326, 1978.
5. **Crawford MH, Souchek J, Oprian CA, Miller DC, Rahimtoola SH, Giacomini JC, Sethi G, Hammermeister KE.** Determinants of survival and left ventricular performance after mitral valve replacement. *Circulation* 81: 1173–1181, 1990.
6. **Dumesnil JG, Honos GN, Lemieux M, Beauchemin J.** Validation and application of indexed aortic prosthetic valve areas calculated by Doppler echocardiography. *J Am Coll Cardiol* 16: 637–643, 1990.
7. **Dumesnil JG, Honos GN, Lemieux M, Beauchemin J.** Validation and applications of mitral prosthetic valvular areas calculated by Doppler echocardiography. *Am J Cardiol* 65: 1443–1448, 1990.
8. **Dumesnil JG, Yoganathan AP.** Valve prosthesis hemodynamics and the problem of high transprosthetic pressure gradients. *Eur J Cardiothorac Surg* 6: S34–S38, 1992.
9. **Enriquez-Sarano M, Schaff HV, Orszulak TA, Tajik AJ, Bailey KR, Frye RL.** Valve repair improves the outcome of surgery for mitral regurgitation. A multivariate analysis. *Circulation* 91: 1022–1028, 1995.
10. **Finkelhor RS, Yang SX, Bosich G, Bahler RC.** Unexplained pulmonary hypertension is associated with systolic arterial hypertension in patients undergoing routine Doppler echocardiography. *Chest* 123: 71–715, 2003.

11. **Flachskampf FA, Rodriguez L, Chen C, Guerrero JL, Weyman AE, Thomas JD.** Analysis of mitral inertance: a factor critical for early transmitral filling. *J Am Soc Echocardiogr* 6: 422–432, 1993.
12. **Gamra H, Zhang HP, Allen JW, Lau FYK, Ruiz CE.** Factors determining normalization of pulmonary vascular resistance following successful balloon mitral valvotomy. *Am J Cardiol* 83: 392–395, 1999.
13. **Garcia D, Barenbrug PJC, Pibarot P, Dekker ALAJ, Van Der Veen FH, Maessen JG, Dumesnil JG, Durand LG.** A ventricular-vascular coupling model in presence of aortic stenosis. *Am J Physiol Heart Circ Physiol* 288: H1874–H1884, 2005.
14. **Garcia D, Pibarot P, Durand LG.** Analytical modeling of the instantaneous pressure gradient across the aortic valve. *J Biomech* 38: 1303–1311, 2005.
15. **Korakianitis T, Shi Y.** Numerical simulation of cardiovascular dynamics with healthy and diseased heart valves. *J Biomech* 39: 1964–1982, 2006.
16. **Lam BK, Chan V, Hendry P, Ruel M, Masters R, Bedard P, Goldstein B, Rubens F, Mesana T.** The impact of patient-prosthesis mismatch on late outcomes after mitral valve replacement. *J Thorac Cardiovasc Surg* 133: 1464–1473, 2007.
17. **Lepeschkin E.** *Modern Electrocardiography*. Baltimore, MD: Williams & Wilkins, 1951.
18. **Levine MJ, Weinstein JS, Diver DJ, Berman AD, Wyman RM, Cunningham MJ, Safian RD, Grossman W, McKay RG.** Progressive improvement in pulmonary vascular resistance after percutaneous mitral valvuloplasty. *Circulation* 79: 1061–1067, 1989.
19. **Li M, Dumesnil JG, Mathieu P, Pibarot P.** Impact of valve prosthesis-patient mismatch on pulmonary arterial pressure after mitral valve replacement. *J Am Coll Cardiol* 45: 1034–1040, 2005.
20. **Lu K, Clark JW, Ghorbel FH, Ware DL, Bidani A.** A human cardiopulmonary system model applied to the analysis of the Vasalva maneuver. *Am J Physiol Heart Circ Physiol* 281: H2661–H2679, 2001.
21. **Magne J, Mathieu P, Dumesnil JG, Tanné D, Dagenais F, Doyle D, Pibarot P.** Impact of prosthesis-patient mismatch on survival after mitral valve replacement. *Circulation* 115: 1417–1425, 2007.
22. **Mahapatra S, Nishimura RA, Sorajja P, Cha S, McGoon MD.** Relationship of pulmonary arterial capacitance and mortality in idiopathic pulmonary arterial hypertension. *J Am Coll Cardiol* 47: 799–803, 2006.
23. **Malouf JF, Enriquez-Sarano M, Bailey KR, Chandrasekaran K, Mullany CJ.** Severe pulmonary hypertension in patients with severe aortic valve stenosis: clinical profile and prognostic implications. *J Am Coll Cardiol* 40: 789–795, 2002.
24. **McLaughlin VV, Rich S.** Pulmonary hypertension. *Curr Probl Cardiol* 29: 575–634, 2004.
25. **Otto CM.** Mitral stenosis. In: *Valvular Heart Disease*. Philadelphia: Saunders, 2004, p. 247–271.
26. **Otto CM, Davis KB, Reid CL, Slater JN, Kronzon I, Kisslo KB, Bashore TM.** Relation between pulmonary artery pressure and mitral stenosis severity in patients undergoing balloon mitral commissurotomy. *Am J Cardiol* 71: 874–878, 1993.
27. **Pibarot P, Dumesnil JG.** Prosthesis-patient mismatch: definition, clinical impact and prevention. *Heart* 92: 1029, 2006.
28. **Pibarot P, Magne J, Dumesnil JG.** Prosthesis-patient mismatch after mitral valve replacement: back to reality. *J Thorac Cardiovasc Surg* 135: 464–465, 2008.
29. **Rahimtoola SH.** The problem of valve prosthesis-patient mismatch. *Circulation* 58: 20–24, 1978.
30. **Sensaki H, Chen CH, Kass DA.** Single-beat estimation of end-systolic pressure-volume relation in humans: a new method with the potential for noninvasive application. *Circulation* 94: 2497–2506, 1996.
31. **Shandas R, Weinberg C, Ivy DD, Nicol E, DeGroff CG, Hertzberg J, Valdes-Cruz L.** Development of a noninvasive ultrasound color M-mode means of estimating pulmonary vascular resistance in pediatric pulmonary hypertension: mathematical analysis, in vitro validation, and preliminary clinical studies. *Circulation* 104: 908–913, 2001.
32. **Sun Y, Beshara M, Lucariello RJ, Chiaramida SA.** A comprehensive model for right-left heart interaction under the influence of pericardium and baroreflex. *Am J Physiol Heart Circ Physiol* 272: H1499–H1515, 1997.
33. **Sun Y, Sjoberg BJ, Ask P, Loyd D, Wranne B.** Mathematical model that characterizes transmitral and pulmonary venous flow velocity patterns. *Am J Physiol Heart Circ Physiol* 268: H476–H489, 1995.
34. **Szabo G, Soans D, Graf A, Beller CJ, Waite L, Hagl S.** A new computer model of mitral valve hemodynamics during ventricular filling. *Eur J Cardiothorac Surg* 26: 239–247, 2004.
35. **Thomas JD, Zhou J, Greenberg N, Bibawy G, McCarthy PM, Vandervoort PM.** Physical and physiological determinants of pulmonary venous flow: numerical analysis. *Am J Physiol Heart Circ Physiol* 272: H2453–H2465, 1997.
36. **Totaro P, Argano V.** Patient-prosthesis mismatch after mitral valve replacement: myth or reality? *J Thorac Cardiovasc Surg* 134: 697–701, 2007.
37. **Tryka AF, Godleski JJ, Schoen FJ, Vandevanter SH.** Pulmonary vascular disease and hypertension after valve surgery for mitral stenosis. *Hum Pathol* 16: 65–71, 1985.
38. **Vandervoort PM, Greenberg N, Pu M, Powell KA, Cosgrove DM, Thomas JD.** Pressure recovery in bileaflet heart valve prostheses: localized high velocities and gradients in central and side orifices with implications for Doppler-catheter gradient relation in aortic and mitral position. *Circulation* 92: 3464–3472, 1995.
39. **Zielinski T, Pogorzelska H, Rajecka A, Biedermavn A.** Pulmonary hemodynamics at rest and effort, 6 and 12 mo after mitral valve replacement: a slow regression of effort pulmonary hypertension. *Int J Cardiol* 42: 57–62, 1993.